1040-5488/12/8905-0543/0 VOL. 89, NO. 5, PP. E543–E553
OPTOMETRY AND VISION SCIENCE

FEATURE REVIEW ON LINE

Clinical Application of Ocular Imaging

Zach Nadler*, Gadi Wollstein†, Hiroshi Ishikawa†, and Joel S. Schuman†

ABSTRACT

The broadening frontier of technology used in ocular imaging is continuously affecting the landscape of clinical eye care. With each wave of enhanced imaging modalities, the field faces the difficulties of optimally incorporating these devices into the clinic. Ocular imaging devices have been widely incorporated into clinical management after their diagnostic capabilities have been documented in a wide range of ocular disease. In this review, we are presenting the main commercially available devices for imaging of the posterior segment of the eye.
(Optom Vis Sci 2012;89:E543–E553)

Key Words: ocular imaging devices, optical coherence tomography, scanning laser ophthalmoscopy, scanning laser polarimetry

In the past two decades, eye care has seen the emergence of three major technologies for diagnostic imaging of the posterior segment of the eye: Scanning Laser Polarimetry (SLP), Confocal Scanning Laser Ophthalmoscopy (CSLO), and Optical Coherence Tomography (OCT). All three devices provide real time, noninvasive, and high-resolution images of the eye. These devices went through the challenging process of translating technological advances into meaningful, robust, and validated applications that are clinically useful and have become an integral part of clinical eye care management in detecting and monitoring various ocular pathologies. Although each deserves its own separate consideration, this article will serve as an overview of the primary state-of-the-art technologies found in the clinic for imaging the posterior segment of the eye and providing quantitative measurements of the ocular structures. The article will first describe each technology, followed by their applications in monitoring and diagnosing ocular diseases.

Scanning Laser Polarimetry

SLP determines the thickness of nerve tissue by examining the birefringence of polarized light as it is reflected from the eye. The size, orientation, and more specifically the microtubular structure of the nerve fibers cause birefringence of incident light.[1] The projected polarized light is subject to reflected phase delay (retardation), which provides a means to estimate tissue thickness.[2] Because other ocular structures in addition to the retina exhibit birefringence, current commercial devices examine and compensate for corneal and other confounding birefringence by using the radial birefringence of Henle fiber layer in the macula as a reference. This approach substantially reduced the occurrence of atypical retardation pattern that hampered the images at earlier version of this technology. The most recent commercially available SLP device, GDx PRO (Carl Zeiss Meditec, Dublin, CA), uses a diode laser with a wavelength of 785 nm and acquires data from $40 \times 20°$ area of retina. Current scanning pattern starts with scanning of the macular region to determine the proper eye-specific corneal compensation properties, followed by scanning centered on the optic nerve head (ONH). An annulus centered on the ONH is sampled from which the retinal nerve fiber thickness is automatically quantified and reported, both as a thickness map and by the temporal superior nasal inferior temporal thickness measurement and profile (Fig. 1). The measured thickness is compared with normative thickness values and reported as a deviation map where areas with either statistically significant thinning or thickening of the RNFL are highlighted. The machine also provides the nerve fiber index, which is generated by an artificial intelligence algorithm that takes into account multiple variables and reports a value that has been shown to correspond to disease status.[3–6]

Confocal Scanning Laser Ophthalmoscopy

CSLO is a confocal microscopy technique with the advantage of having high transverse resolution. CSLO focuses a beam onto tissue and filters reflecting light from outside the focal point by use of a confocal pinhole situated in front of a photodetector at a focal

*BS
†MD
Department of Ophthalmology, UPMC Eye Center, Eye and Ear Institute, Ophthalmology and Visual Science Research Center, University of Pittsburgh School of Medicine, Pittsburgh, Pennsylvania (ZN, GW, HI, JSS), and Department of Bioengineering, Swanson School of Engineering, University of Pittsburgh, Pittsburgh, Pennsylvania (HI, JSS).

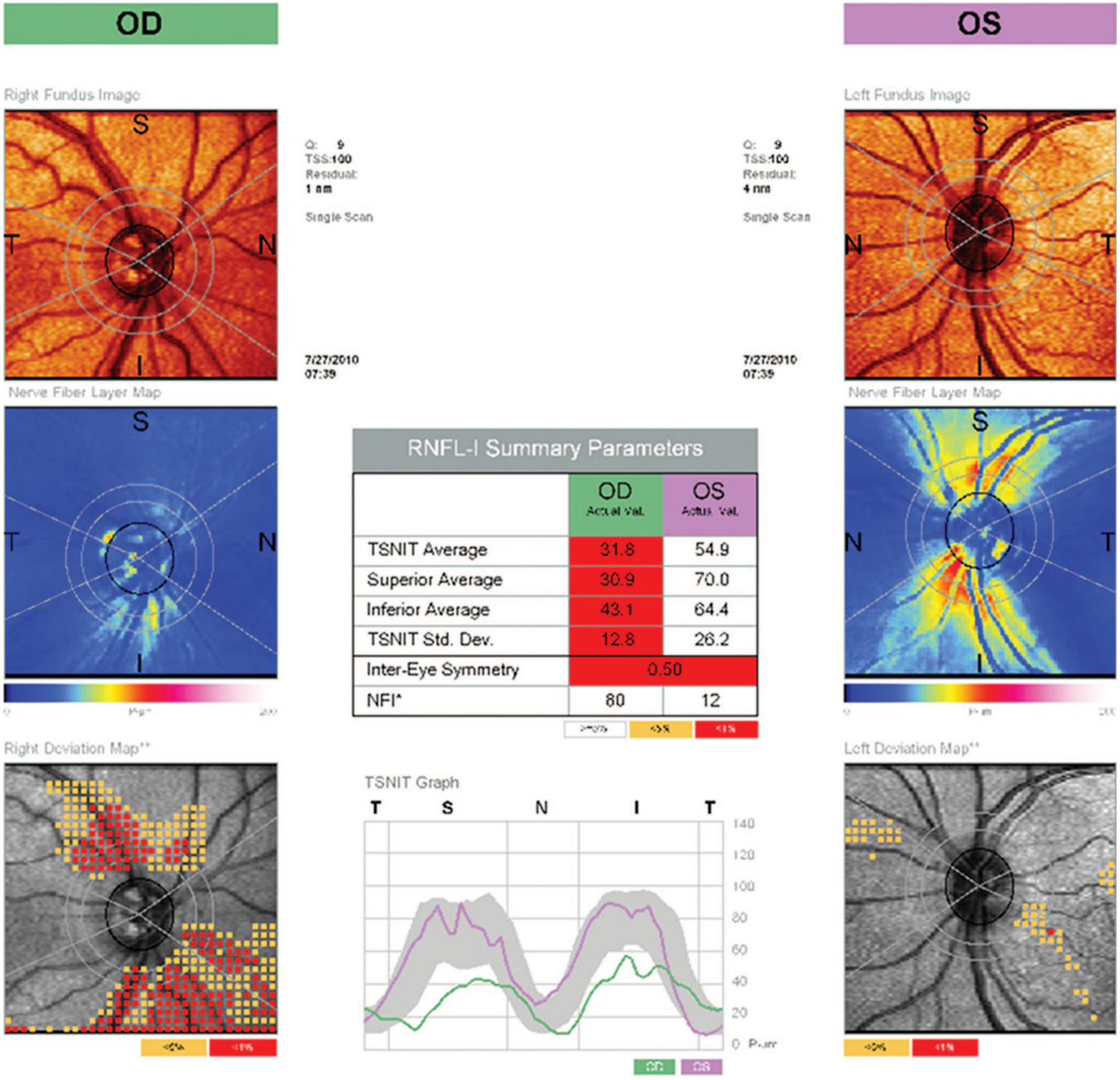

FIGURE 1.

SLP printout with the GDx PRO; the OS has a near normal retinal fiber layer map appearance as evidenced by the thickening (red color) superior and inferior to the optic nerve with a small and early localized thinning at the inferior temporal aspect of the disc noticeable in the deviation map. The OD exhibits extensive thinning in the superior and inferior regions, marked by red and yellow indicators in the deviation map. The center table contains the quantitative measurements with the color coded comparison with normative database. Figs. 1 to 3 were all acquired from the same subject using different imaging devices. A color version of this figure is available online at www.optvissci.com.

conjugate. The commercially available CSLO device, Heidelberg Retina Tomography III (HRT III; Heidelberg Engineering, Heidelberg, Germany) uses a diode laser beam with a wavelength of 670 nm and captures a series of evenly spaced 16 to 64 sequential 2-dimensional frames each covering an area of 15 × 15°. The optical transverse resolution of the HRT is 10 μm and the axial resolution is 300 μm. The initial scans are focused anterior to the retina and the last scans are posterior to the bottom of the optic cup, and the depth of ONH dictates the number of frames. For each focal plane, the HRT acquires 384 × 384 samplings that records a reflection intensity value at each of the particular (x, y) coordinates of the focal plane. For each (x, y) point, the machine determines the surface location in the z axis derived from the center of gravity of the reflected light along the frames. Three sets of scans are acquired in a rapid succession and aligned, and the average of the three scans is used for the analysis. The operator is required to trace the ONH margin and accordingly the device automatically defines a reference plane to differentiate between the cup and the neuroretinal rim structures. The acquired scans are summarized as a reflectance image resembling the clinical view of the ONH region

along with topographic map overlaid with the cup and disc boundaries (Fig. 2). In addition, the machine provides numerous parameters that quantify the ONH region. HRT III also provides another method for analyzing the ONH structure without the need of manual delineation of the optic disc margin. This method, the Glaucoma Probability Score, is based on fitting a predefined model of the ONH region and provides global and sectoral quantification of the region.[7]

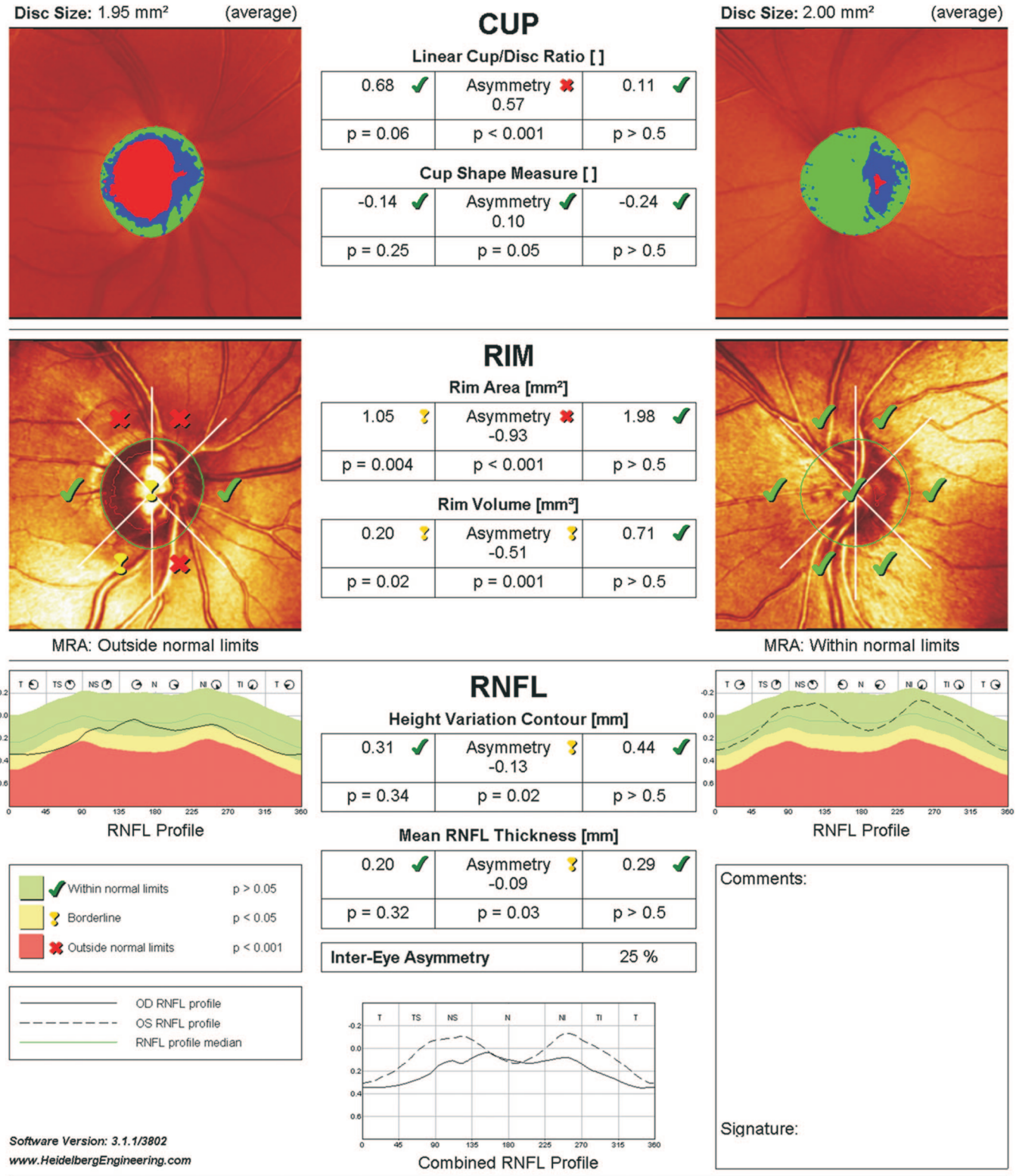

FIGURE 2.

CSLO printout of the HRTIII with quantitative parameters shown in the center. The OD shows signs of glaucomatous damage as highlighted by the red and yellow warning markings on the reflectance image shown in the center. The topography image (uppermost) demonstrates enlarged ONH cupping marked by the red color. The OS falls within the normal limits. A color version of this figure is available online at www.optvissci.com.

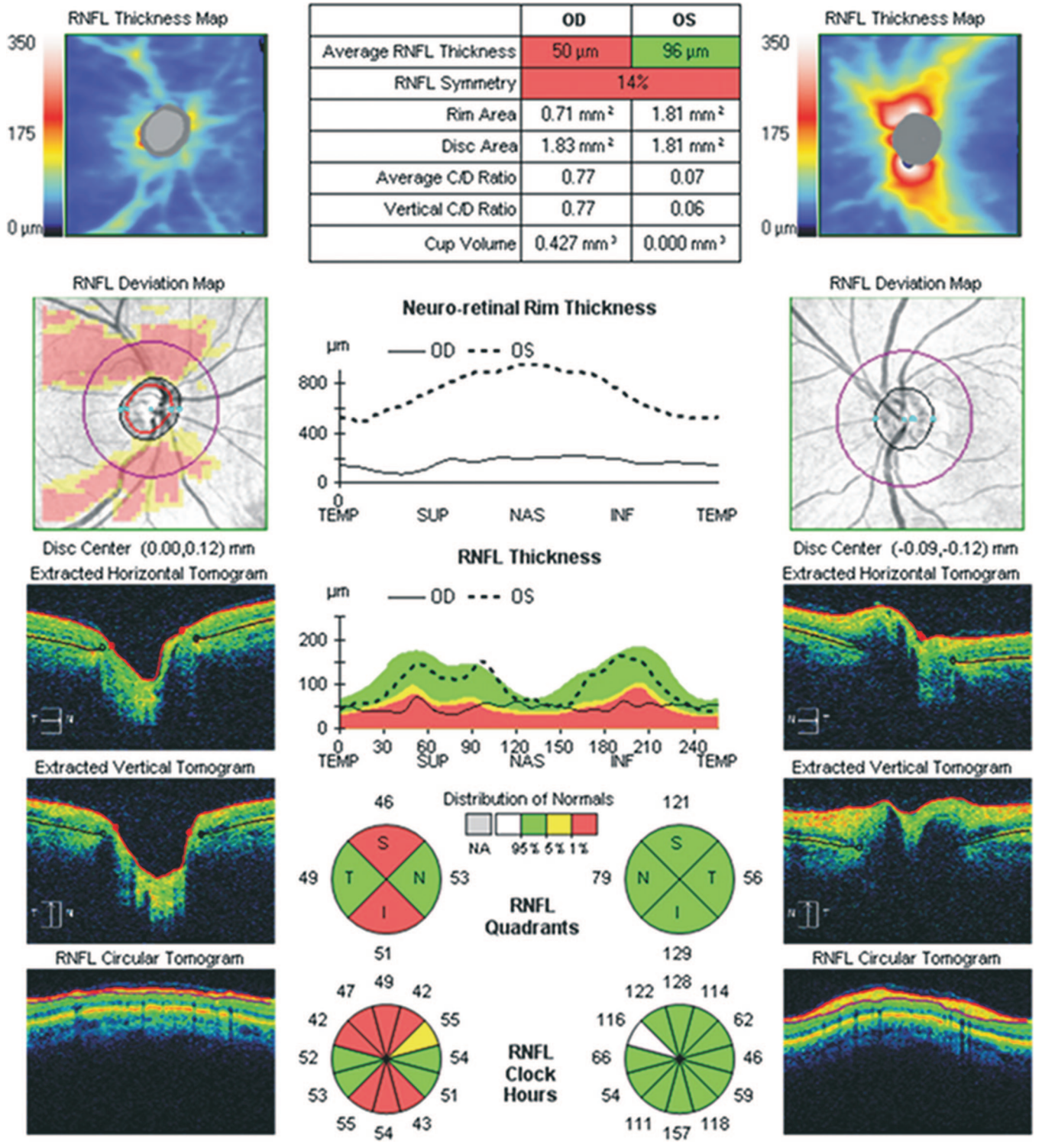

FIGURE 3.

ONH and RNFL printout from Cirrus SD OCT. The OS shows normal RNFL thickness map with thickening adjacent to the ONH poles. The OD exhibits extensive thinning of the RNFL in the superior and inferior regions in the RNFL thickness map. The thinning is noticeable by the large area of significant thinning at the RNFL deviation map. Quantitative parameters of the ONH and RNFL appear at the top center with color coded comparison with normative dataset. Quadrant and 1-o'clock hour RNFL thickness and RNFL thickness profiles are provided at the center bottom. A color version of this figure is available online at www.optvissci.com.

Optical Coherence Tomography

OCT uses low-coherence interferometry, where backscattered light is interfered with a reference beam to create an axial scan (A-scan) of depth resolved tissue reflectivity. Consecutive beams are scanned transversely to recreate a cross-sectional slice of scattering media (B-scan).[8] Initially, OCT was conducted in the time domain (TD OCT), where a reference mirror was moved to acquire a depth reflectivity profile for a particular locale in the tissue.

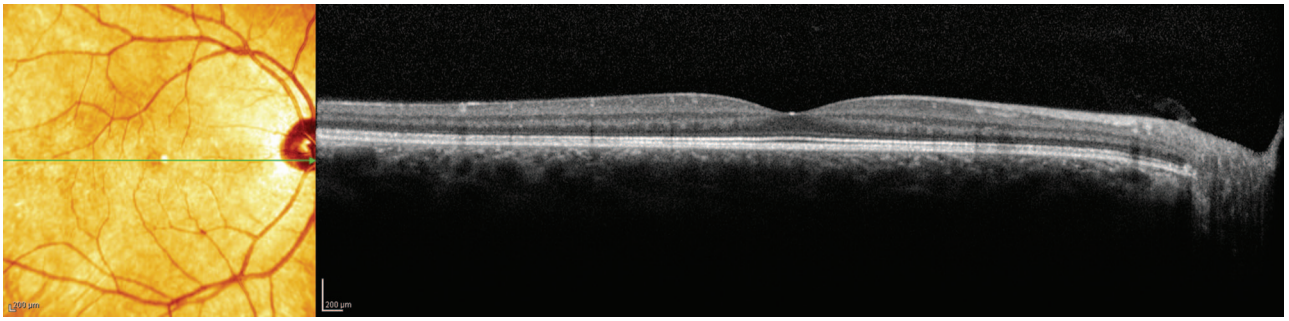

FIGURE 4.

Cross-sectional (B-scan) image taken with the Spectralis. The green line in the fundus image on the left represents the placement of the OCT scan extending through the entire macula and most of the ONH. The layered pattern of the retina is clearly evident in the image. A color version of this figure is available online at www.optvissci.com.

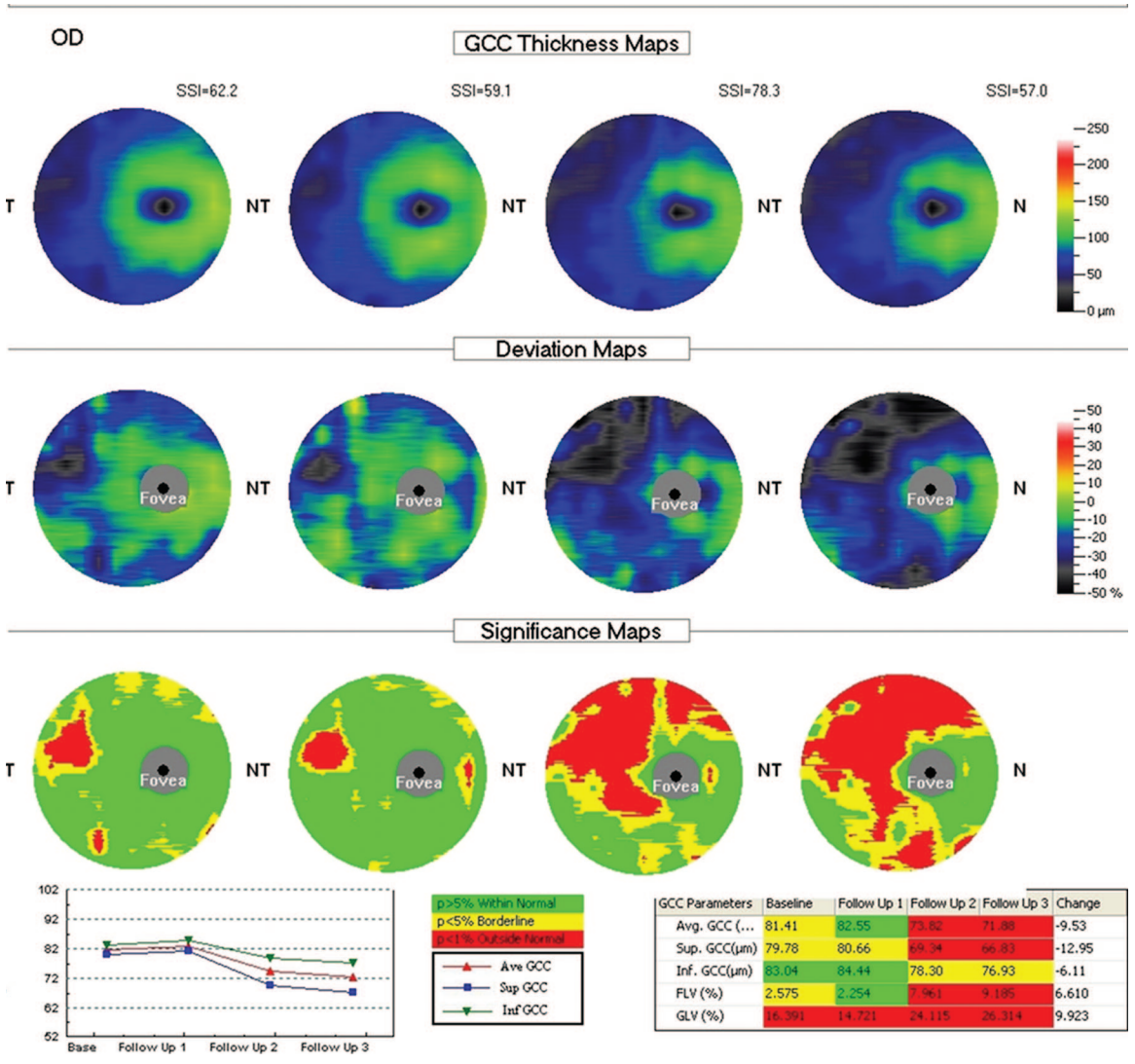

FIGURE 5.

Ganglion cell complex (GCC) thickness and deviation map for a progressing glaucomatous eye taken with RTVue. The top row contains the overall thickness map, progressing longitudinally from left to right with thickness values indicated by the adjacent color bar. The middle row shows a deviation of thickness from normal. The significance map at the bottom highlights regions of statistically significant thinning of the GCC. The defect starts as a localized region temporally, and over time progresses nasally occupying most of the superior region, and eventually extending inferiorly. A color version of this figure is available online at www.optvissci.com.

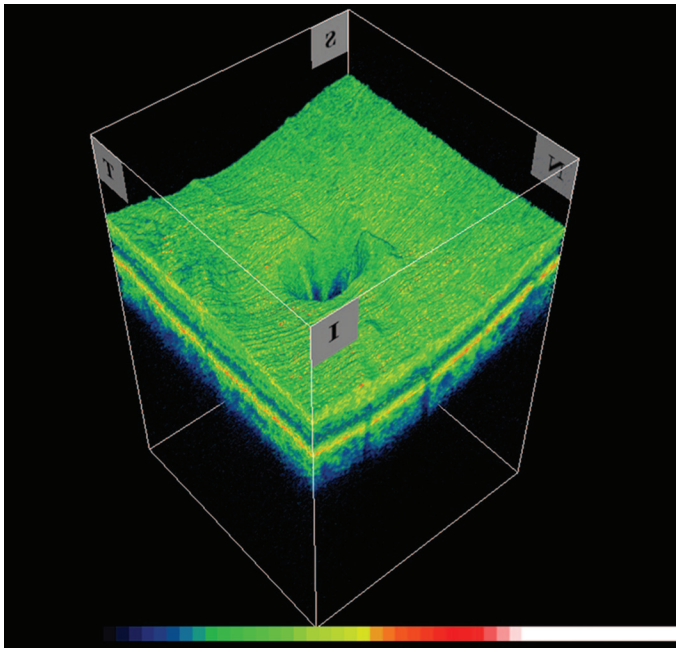

FIGURE 6.
Three-dimensional reconstruction of the ONH morphology by the Topcon 3-D OCT 2000. Cross-section maps occur at the margin of the cube. A color version of this figure is available online at www.optvissci.com.

The physical limitation of a moving reference mirror restricts the speed of TD-OCT systems to ~400 A-scans/s. To limit the deleterious effect of eye movements, corneal dryness, and blinking, the available scanning patterns were limited to a circumpapillary scan or six radial slices in a spoke configuration centered on either the macula or the ONH. More recently, spectral domain OCT (SD OCT) has been introduced eliminating the need of physically moving mirror, the device samples broad spectral information for a particular location in the tissue. By Fourier transforming the power spectra, it is able to recover tissue reflectivity information. SD OCT uses a spectrometer and charge-coupled-device camera to separate and detect the spectrally resolved signal.[9] With the dramatic increase in speed and axial resolution afforded by SD OCT over TD OCT, a full 3-dimensional volumetric imaging reconstructed from rapid raster scan patterns can be obtained.[10]

Several SD OCT commercial devices are currently available, each offering their own distinct advantages. Most operate at a speed around 27,000 A-scans/s, with a current maximum of 52,000 A-scans/s (SOCT Copernicus; Optopol, Miami, FL). Axial resolutions range from 3 μm (SOCT Copernicus), 3.9 μm (Spectralis; Heidelberg Engineering; Fig. 3), and 4 μm (Bioptigen SDOIS; Bioptigen, Durham, NC) to 6 μm (Spectral OCT SLO, OPKO Health, Miami, FL). Cirrus HD OCT (Carl Zeiss Meditec; Fig. 4), RTVue-100 (Optovue, Fremont, CA; Fig. 5), and SOCT Copernicus, all include progression analysis software for monitoring pathologies. The Bioptigen device is more geared toward research and permits user control over the scanning protocol. Some devices incorporate features of other imaging modalities: the 3-D OCT 2000 device (Topcon, Tokyo, Japan; Fig. 6) has a built in high-resolution fundus camera for improved registration. The OPKO device includes an SLO image and microperimetry. The Spectralis device includes eye tracking, and SLO coupled with fluorescein angiography, and autofluorescence in addition to the OCT system. The autofluorescence uses a 488 nm wavelength light source to illuminate the retina, inducing fluorescence without injecting dye. This highlight structures such as drusens and improve the ability of detecting these structures. It should be noted that both fluorescein angiography and autofluorescence lack the quantitative analysis characteristic of the other modes but are clinically useful for visualizing retinal pathologies.

The parameters provided vary among the devices though most report the retinal nerve fiber layer (RNFL) thickness globally and in sectors. Macula scans are typically quantified by the total retinal thickness or volume, and some devices provide further segmentation of the macular layers (Cirrus and RTVue).

Imaging Pathologies

The imaging technologies outlined above provide a detailed view and structural quantitative measures at the posterior segment of the eye. Considering their attributes, the most prominent use of the ophthalmic imaging devices is for retinal diseases and glaucoma. The enhanced visualization has been shown to be of important diagnostic value in diabetic macular edema, age-related macular degeneration (AMD; Fig. 7), macular hole (Fig. 8), vitreomacular traction, epiretinal membrane, and others.[11–15] Hard drusen, a hallmark of AMD, appears as highly reflective deposits underneath the retinal pigment epithelium layer, in OCT scans. The number and size of the drusen can be quantified by OCT and has been shown to be associated with the risk of AMD.[16–19] Ocular imaging devices have been used for grading macular holes and accordingly dictate the preferred surgical approach.[20–23] Similarly, the ability to visualize the epiretinal membrane and vitreomacular traction strand assist in determining the surgical approach and treatment outcome.[24–27] The devices have also been valuable in assessing central serous chorioretinopathy without the need of invasive testing such as fluorescein angiography.[11] In some instances, the break of the retinal pigment epithelium through which the leakage occur could be detected by OCT.[28] Consecutive imaging allows tracing the longitudinal dynamic of the serous collection and treatment response. The ability to quantify the retinal thickness is of use in assessing pathologies such as macular edema and the response to treatment.[29,30] These examples illustrate some of the clinical uses of the imaging devices from a wide array of indications. Recently, an automated method of classifying macular hole, macular edema, and AMD has been shown to successfully identify these macular pathologies.[31]

Ocular imaging devices have become pivotal in clinical glaucoma assessment because of their ability of obtaining micron scale measurements. Glaucoma is a slow progressing and irreversible neurodegenerative disease that remains mostly asymptomatic until late stages. The disease manifests as the thinning of retinal layers and cupping of the ONH. The devices have been shown to provide highly reproducible measurements of the RNFL and ONH structures.[32–42] These measurements can quantify the thinning of the RNFL, the typical enlargement of the optic disc cup and the thinning of the neuroretinal rim. The improved segmentation ability of recent iteration of the OCT allows the quantification of the mac-

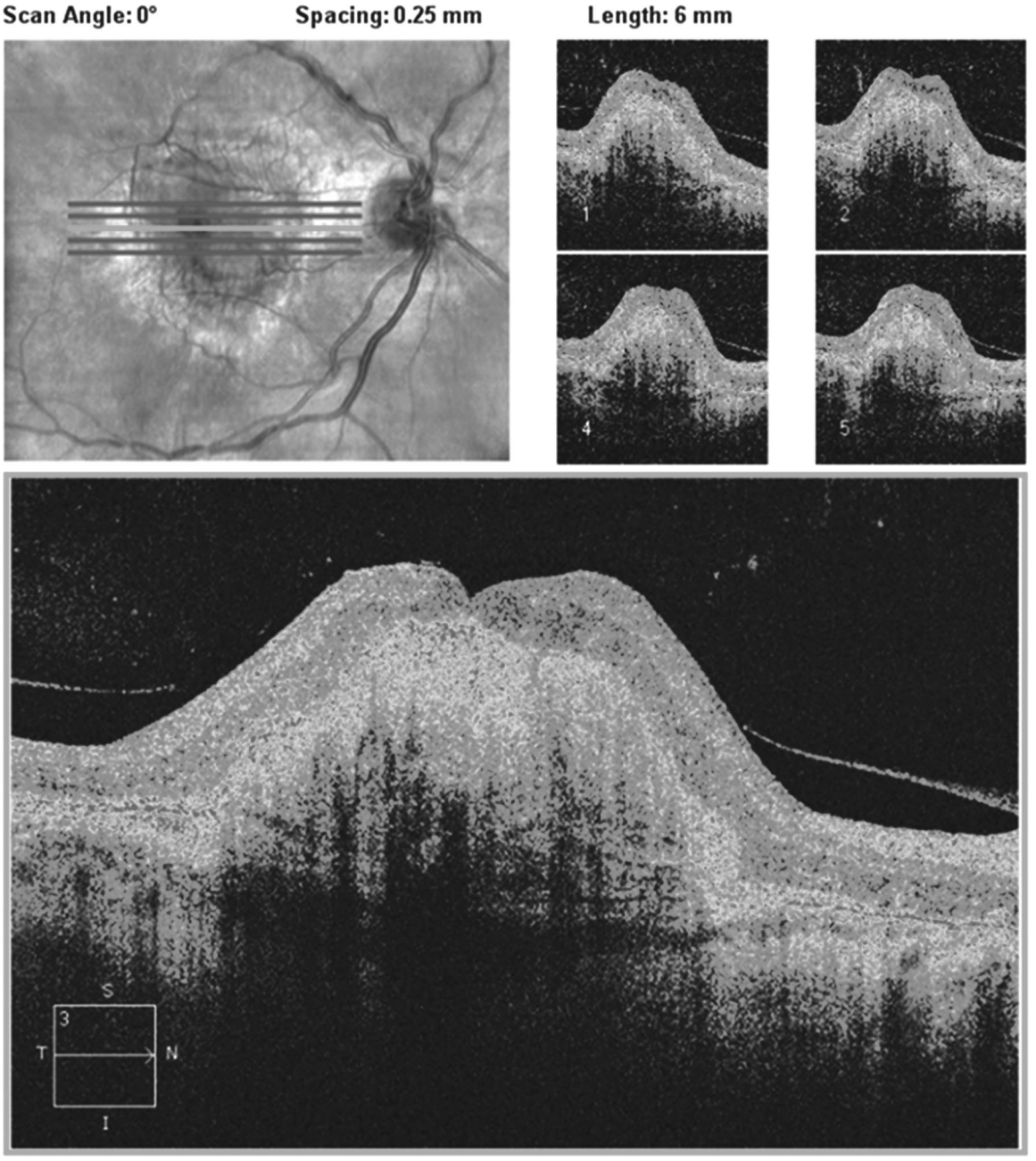

FIGURE 7.

High definition raster scan printout of AMD from the Cirrus HD OCT. The scan includes five linear scans (top left) with the center scan magnified at the bottom. Marked elevation of the foveal region is evident with irregularity at the retinal pigment epithelium photoreceptor layer. A color version of this figure is available online at www.optvissci.com.

ular ganglion cell layer, which has been shown to be an alternative sampling location for glaucoma diagnosis.[43–46] Numerous studies have demonstrated good discrimination ability of the devices between healthy and glaucomatous eyes.[47–53] Using cross-sectional data, it has been shown that in early stages of glaucoma, thinning of the RNFL thickness, as measured by OCT, occurs without changes in visual field as measured by current technology.[54] After reaching a threshold level, there is a decline by both structure and function, which might indicate that structural changes precede functional changes in some glaucoma patients further emphasizing the benefit of ocular imaging devices. Furthermore, baseline HRT and GDx measurements have been demonstrated to predict future development of glaucomatous visual field damage.[4,55–57] Taken together, the important role of ophthalmic imaging devices in glaucoma assessment has been widely accepted.

Longitudinal Studies

A focal point of clinical research is understanding the trajectory a pathology takes in an individual subject. One of the most powerful means of examining this is a longitudinal study, where subjects are followed-up over an extended period of time. However, longitudinal studies of clinical subjects are laced with difficulty. Diseases can be slow progressing, and the technology

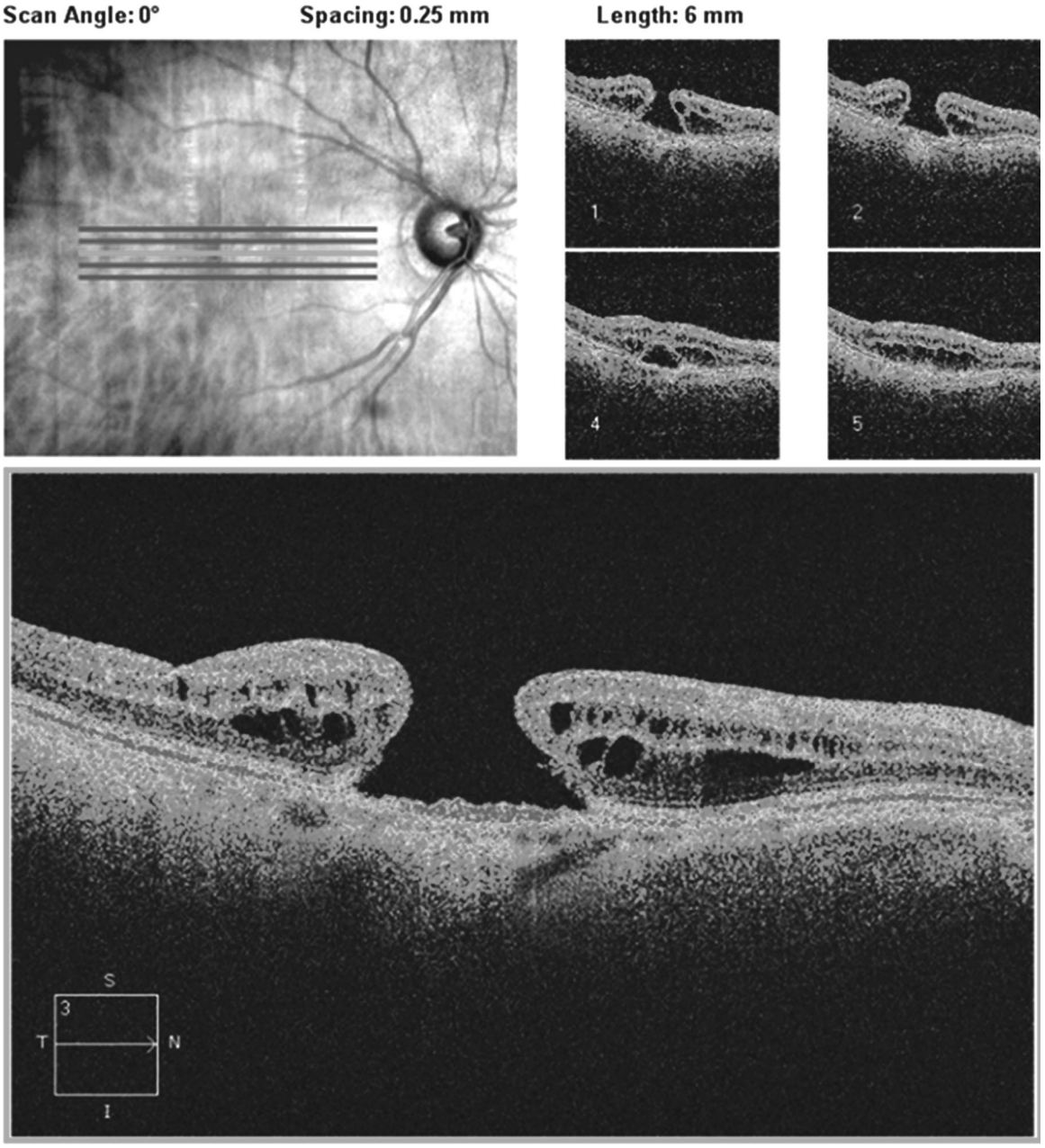

FIGURE 8.

High definition raster scan printout of macular hole from the Cirrus HD OCT. Full-thickness hole with intraretinal edema at the hole margin occurring as the black spaces are clearly visible. A color version of this figure is available online at www.optvissci.com.

involved in data acquisition is imperfect and constantly changing. Comparing scans longitudinally requires registration of spatially coincident information collected at different time points. The great challenge of rapidly evolving technology is maintaining congruence by finding ways to translate between generations so that past data can be still used. Furthermore, numerous manufacturers are currently available for OCT, yet no standard of scan patterns or analysis was established, and therefore measurements obtained with one OCT instrument are not interchangeable with measurements obtained from an instrument manufactured by another company. At the time of writing this review, there is no universal reader for OCT that can be used with all available devices.

In many retinal diseases, the ability to obtain consecutive highly detailed visualization over time is sufficient for qualitative assessment of the disease process. For example, the disappearance of retinal puckers after peeling of epiretinal membrane will be evaluated by visualizing the images. However, in many instances, precise quantification of the changes occurring along the disease process is desirable. Because of the high reproducibility of the measurements obtained by optical imaging devices, any change exceeding the inherent measurement variability might be attributed to the disease process. HRT defines the measurements variability for each eye by assessing the difference between several baseline images and accordingly sets the limit for any follow-up image.[58] Other technologies use the variability as recorded in population-based studies.

This method is often described as an event analysis, and it is mainly useful for situations where changes are expected to occur in a stepwise manner or in acute events. Another approach, called trend analysis, is based on computing the slope of change over time either by a regression analysis or Bayesian analysis.[59] A slope that statistically significantly exceeds the rate of zero change is marked or when the rate of progression exceeds the normal age related rate of change. This method is mostly suitable for situations where the disease is progressing in a homogenous or continuous pattern. A few studies have shown that the ocular imaging devices are capable of detecting changes over time in healthy and glaucomatous subjects.[60–62] However, the correspondence between progression as detected by visual field and imaging devices in various glaucoma studies was limited, as was the agreement on progression between the various devices.[61–63] These results might be explained either by the different time scale for structure and function progression or by the different physical properties of the various devices that might be suitable for disease detection in different stages of the disease. Further studies with larger cohorts and longer period of follow-up are needed to fully elucidate the role of imaging devices in longitudinal assessment in glaucoma.

CONCLUSIONS

The current forefront of technological advancement in ocular imaging plays a major role in clinical assessment and monitoring of the posterior segment of the eye. Clinical studies evaluating current commercial technology have demonstrated the ability to proficiently detect disease. However, characterizing the trajectory of a disease felt by individuals remains incomplete. The rapid evolution of the imaging devices hold promise for further strengthening of their roles in clinical practice.

ACKNOWLEDGMENTS

This research was supported in part by National Eye Institute, National Institutes of Health contracts R01-EY013178, R01-EY013516, and P30-EY008098 (Bethesda, MD); Eye and Ear Foundation (Pittsburgh, PA); and unrestricted grants from Research to Prevent Blindness (New York, NY).

Dr. Schuman received royalties for intellectual property licensed by Massachusetts Institute of Technology to Carl Zeiss Meditec.

Received October 11, 2011; accepted December 16, 2011.

REFERENCES

1. Huang XR, Knighton RW. Microtubules contribute to the birefringence of the retinal nerve fiber layer. Invest Ophthalmol Vis Sci 2005;46:4588–93.
2. Weinreb RN, Shakiba S, Zangwill L. Scanning laser polarimetry to measure the nerve fiber layer of normal and glaucomatous eyes. Am J Ophthalmol 1995;119:627–36.
3. Reus NJ, Lemij HG. Diagnostic accuracy of the GDx VCC for glaucoma. Ophthalmology 2004;111:1860–5.
4. Da Pozzo S, Iacono P, Marchesan R, Fantin A, Ravalico G. Scanning laser polarimetry with variable corneal compensation and detection of glaucomatous optic neuropathy. Graefes Arch Clin Exp Ophthalmol 2005;243:774–9.
5. Iester M, Perdicchi A, De Feo F, Fiesoletti E, Amodeo S, Sanna G, Leonardi A, Calabria G. Comparison between GDx VCC parameter and achromatic perimetry in glaucoma patients. J Glaucoma 2006; 15:281–5.
6. Medeiros FA, Vizzeri G, Zangwill LM, Alencar LM, Sample PA, Weinreb RN. Comparison of retinal nerve fiber layer and optic disc imaging for diagnosing glaucoma in patients suspected of having the disease. Ophthalmology 2008;115:1340–6.
7. Swindale NV, Stjepanovic G, Chin A, Mikelberg FS. Automated analysis of normal and glaucomatous optic nerve head topography images. Invest Ophthalmol Vis Sci 2000;41:1730–42.
8. Huang D, Swanson EA, Lin CP, Schuman JS, Stinson WG, Chang W, Hee MR, Flotte T, Gregory K, Puliafito CA, Fujimoto JG. Optical coherence tomography. Science 1991;254:1178–81.
9. Drexler W, Fujimoto JG. State-of-the-art retinal optical coherence tomography. Prog Retin Eye Res 2008;27:45–88.
10. Wojtkowski M, Srinivasan V, Fujimoto JG, Ko T, Schuman JS, Kowalczyk A, Duker JS. Three-dimensional retinal imaging with high-speed ultrahigh-resolution optical coherence tomography. Ophthalmology 2005;112:1734–46.
11. Drexler W, Sattmann H, Hermann B, Ko TH, Stur M, Unterhuber A, Scholda C, Findl O, Wirtitsch M, Fujimoto JG, Fercher AF. Enhanced visualization of macular pathology with the use of ultrahigh-resolution optical coherence tomography. Arch Ophthalmol 2003;121:695–706.
12. Srinivasan VJ, Wojtkowski M, Witkin AJ, Duker JS, Ko TH, Carvalho M, Schuman JS, Kowalczyk A, Fujimoto JG. High-definition and 3-dimensional imaging of macular pathologies with high-speed ultrahigh-resolution optical coherence tomography. Ophthalmology 2006;113:2054.e1–14.
13. Huang LL, Levinson DH, Levine JP, Mian U, Tsui I. Optical coherence tomography findings in idiopathic macular holes. J Ophthalmol 2011;2011:928205.
14. Gallemore RP, Jumper JM, McCuen BW, II, Jaffe GJ, Postel EA, Toth CA. Diagnosis of vitreoretinal adhesions in macular disease with optical coherence tomography. Retina 2000;20:115–20.
15. Ko TH, Fujimoto JG, Schuman JS, Paunescu LA, Kowalevicz AM, Hartl I, Drexler W, Wollstein G, Ishikawa H, Duker JS. Comparison of ultrahigh- and standard-resolution optical coherence tomography for imaging macular pathology. Ophthalmology 2005;112: 1922.e1–15.
16. Schuman SG, Koreishi AF, Farsiu S, Jung SH, Izatt JA, Toth CA. Photoreceptor layer thinning over drusen in eyes with age-related macular degeneration imaged in vivo with spectral-domain optical coherence tomography. Ophthalmology 2009;116:488–96.
17. Chen Y, Vuong LN, Liu J, Ho J, Srinivasan VJ, Gorczynska I, Witkin AJ, Duker JS, Schuman J, Fujimoto JG. Three-dimensional ultrahigh resolution optical coherence tomography imaging of age-related macular degeneration. Opt Express 2009;17:4046–60.
18. Yi K, Mujat M, Park BH, Sun W, Miller JW, Seddon JM, Young LH, de Boer JF, Chen TC. Spectral domain optical coherence tomography for quantitative evaluation of drusen and associated structural changes in non-neovascular age-related macular degeneration. Br J Ophthalmol 2009;93:176–81.
19. Freeman SR, Kozak I, Cheng L, Bartsch DU, Mojana F, Nigam N, Brar M, Yuson R, Freeman WR. Optical coherence tomography-raster scanning and manual segmentation in determining drusen volume in age-related macular degeneration. Retina 2010;30:431–5.
20. Inoue M, Watanabe Y, Arakawa A, Sato S, Kobayashi S, Kadonosono K. Spectral-domain optical coherence tomography images of inner/outer segment junctions and macular hole surgery outcomes. Graefes Arch Clin Exp Ophthalmol 2009;247:325–30.
21. Michalewska Z, Michalewski J, Cisiecki S, Adelman R, Nawrocki J. Correlation between foveal structure and visual outcome following

macular hole surgery: a spectral optical coherence tomography study. Graefes Arch Clin Exp Ophthalmol 2008;246:823–30.
22. Oh J, Smiddy WE, Flynn HW, Jr., Gregori G, Lujan B. Photoreceptor inner/outer segment defect imaging by spectral domain OCT and visual prognosis after macular hole surgery. Invest Ophthalmol Vis Sci 2010;51:1651–8.
23. Ip MS, Baker BJ, Duker JS, Reichel E, Baumal CR, Gangnon R, Puliafito CA. Anatomical outcomes of surgery for idiopathic macular hole as determined by optical coherence tomography. Arch Ophthalmol 2002;120:29–35.
24. Chang LK, Fine HF, Spaide RF, Koizumi H, Grossniklaus HE. Ultrastructural correlation of spectral-domain optical coherence tomographic findings in vitreomacular traction syndrome. Am J Ophthalmol 2008;146:121–7.
25. Koizumi H, Spaide RF, Fisher YL, Freund KB, Klancnik JM, Jr., Yannuzzi LA. Three-dimensional evaluation of vitreomacular traction and epiretinal membrane using spectral-domain optical coherence tomography. Am J Ophthalmol 2008;145:509–17.
26. Mojana F, Cheng L, Bartsch DU, Silva GA, Kozak I, Nigam N, Freeman WR. The role of abnormal vitreomacular adhesion in age-related macular degeneration: spectral optical coherence tomography and surgical results. Am J Ophthalmol 2008;146:218–27.
27. Uchino E, Uemura A, Doi N, Ohba N. Postsurgical evaluation of idiopathic vitreomacular traction syndrome by optical coherence tomography. Am J Ophthalmol 2001;132:122–3.
28. Fujimoto H, Gomi F, Wakabayashi T, Sawa M, Tsujikawa M, Tano Y. Morphologic changes in acute central serous chorioretinopathy evaluated by fourier-domain optical coherence tomography. Ophthalmology 2008;115:1494–500.
29. Hatef E, Colantuoni E, Wang J, Ibrahim M, Shulman M, Adhi F, Sepah YJ, Channa R, Khwaja A, Nguyen QD, Do DV. The relationship between macular sensitivity and retinal thickness in eyes with diabetic macular edema. Am J Ophthalmol 2011;152:400–5.
30. Virgili G, Menchini F, Murro V, Peluso E, Rosa F, Casazza G. Optical coherence tomography (OCT) for detection of macular oedema in patients with diabetic retinopathy. Cochrane Database Syst Rev 2011(7):CD008081.
31. Liu YY, Ishikawa H, Chen M, Wollstein G, Duker JS, Fujimoto JG, Schuman JS, Rehg JM. Computerized macular pathology diagnosis in spectral domain optical coherence tomography scans based on multiscale texture and shape features. Invest Ophthalmol Vis Sci 2011;52:8316–22.
32. Budenz DL, Chang RT, Huang X, Knighton RW, Tielsch JM. Reproducibility of retinal nerve fiber thickness measurements using the stratus OCT in normal and glaucomatous eyes. Invest Ophthalmol Vis Sci 2005;46:2440–3.
33. Strouthidis NG, Demirel S, Asaoka R, Cossio-Zuniga C, Garway-Heath DF. The Heidelberg retina tomograph Glaucoma Probability Score: reproducibility and measurement of progression. Ophthalmology 2010;117:724–9.
34. DeLeon Ortega JE, Sakata LM, Kakati B, McGwin G, Jr., Monheit BE, Arthur SN, Girkin CA. Effect of glaucomatous damage on repeatability of confocal scanning laser ophthalmoscope, scanning laser polarimetry, and optical coherence tomography. Invest Ophthalmol Vis Sci 2007;48:1156–63.
35. Ng D, Zangwill LM, Racette L, Bowd C, Pascual JP, Bourne RR, Boden C, Weinreb RN, Sample PA. Agreement and repeatability for standard automated perimetry and confocal scanning laser ophthalmoscopy in the diagnostic innovations in glaucoma study. Am J Ophthalmol 2006;142:381–6.
36. Garas A, Toth M, Vargha P, Hollo G. Comparison of repeatability of retinal nerve fiber layer thickness measurement made using the RTVue Fourier-domain optical coherence tomograph and the GDx scanning laser polarimeter with variable or enhanced corneal compensation. J Glaucoma 2010;19:412–7.
37. Mai TA, Reus NJ, Lemij HG. Retinal nerve fiber layer measurement repeatability in scanning laser polarimetry with enhanced corneal compensation. J Glaucoma 2008;17:269–74.
38. Krebs I, Smretschnig E, Moussa S, Brannath W, Womastek I, Binder S. Quality and reproducibility of retinal thickness measurements in two spectral-domain optical coherence tomography machines. Invest Ophthalmol Vis Sci 2011;52:6925–33.
39. Langenegger SJ, Funk J, Toteberg-Harms M. Reproducibility of retinal nerve fiber layer thickness measurements using the eye tracker and the retest function of Spectralis SD-OCT in glaucomatous and healthy control eyes. Invest Ophthalmol Vis Sci 2011;52:3338–44.
40. Mwanza JC, Chang RT, Budenz DL, Durbin MK, Gendy MG, Shi W, Feuer WJ. Reproducibility of peripapillary retinal nerve fiber layer thickness and optic nerve head parameters measured with cirrus HD-OCT in glaucomatous eyes. Invest Ophthalmol Vis Sci 2010; 51:5724–30.
41. Garas A, Vargha P, Hollo G. Reproducibility of retinal nerve fiber layer and macular thickness measurement with the RTVue-100 optical coherence tomograph. Ophthalmology 2010;117:738–46.
42. Menke MN, Dabov S, Knecht P, Sturm V. Reproducibility of retinal thickness measurements in patients with age-related macular degeneration using 3D Fourier-domain optical coherence tomography (OCT) (Topcon 3D-OCT 1000). Acta Ophthalmol 2011;89: 346–51.
43. Ishikawa H, Stein DM, Wollstein G, Beaton S, Fujimoto JG, Schuman JS. Macular segmentation with optical coherence tomography. Invest Ophthalmol Vis Sci 2005;46:2012–7.
44. Mwanza JC, Oakley JD, Budenz DL, Chang RT, Knight OJ, Feuer WJ. Macular ganglion cell-inner plexiform layer: automated detection and thickness reproducibility with spectral domain-optical coherence tomography in glaucoma. Invest Ophthalmol Vis Sci 2011; 52:8323–9.
45. Tan O, Chopra V, Lu AT, Schuman JS, Ishikawa H, Wollstein G, Varma R, Huang D. Detection of macular ganglion cell loss in glaucoma by Fourier-domain optical coherence tomography. Ophthalmology 2009;116:2305–14.
46. Guedes V, Schuman JS, Hertzmark E, Wollstein G, Correnti A, Mancini R, Lederer D, Voskanian S, Velazquez L, Pakter HM, Pedut-Kloizman T, Fujimoto JG, Mattox C. Optical coherence tomography measurement of macular and nerve fiber layer thickness in normal and glaucomatous human eyes. Ophthalmology 2003;110: 177–89.
47. Medeiros FA, Zangwill LM, Bowd C, Weinreb RN. Comparison of the GDx VCC scanning laser polarimeter, HRT II confocal scanning laser ophthalmoscope, and stratus OCT optical coherence tomograph for the detection of glaucoma. Arch Ophthalmol 2004;122: 827–37.
48. Burgansky-Eliash Z, Wollstein G, Bilonick RA, Ishikawa H, Kagemann L, Schuman JS. Glaucoma detection with the Heidelberg retina tomograph 3. Ophthalmology 2007;114:466–71.
49. Wollstein G, Garway-Heath DF, Hitchings RA. Identification of early glaucoma cases with the scanning laser ophthalmoscope. Ophthalmology 1998;105:1557–63.
50. Reddy S, Xing D, Arthur SN, Harizman N, Dorairaj S, Ritch R, Liebmann JM. HRT III glaucoma probability score and Moorfields regression across the glaucoma spectrum. J Glaucoma 2009;18: 368–72.
51. Sung KR, Wollstein G, Schuman JS, Bilonick RA, Ishikawa H, Townsend KA, Kagemann L, Gabriele ML. Scan quality effect on glaucoma discrimination by glaucoma imaging devices. Br J Ophthalmol 2009;93:1580–4.

52. Mai TA, Reus NJ, Lemij HG. Diagnostic accuracy of scanning laser polarimetry with enhanced versus variable corneal compensation. Ophthalmology 2007;114:1988–93.
53. Leite MT, Zangwill LM, Weinreb RN, Rao HL, Alencar LM, Sample PA, Medeiros FA. Effect of disease severity on the performance of Cirrus spectral-domain OCT for glaucoma diagnosis. Invest Ophthalmol Vis Sci 2010;51:4104–9.
54. Wollstein G, Kagemann L, Bilonick RA, Ishikawa H, Folio LS, Gabriele ML, Ungar AK, Duker JS, Fujimoto JG, Schuman JS. Retinal nerve fibre layer and visual function loss in glaucoma: the tipping point. Br J Ophthalmol 2012;96:47–52.
55. Bowd C, Zangwill LM, Medeiros FA, Hao J, Chan K, Lee TW, Sejnowski TJ, Goldbaum MH, Sample PA, Crowston JG, Weinreb RN. Confocal scanning laser ophthalmoscopy classifiers and stereophotograph evaluation for prediction of visual field abnormalities in glaucoma-suspect eyes. Invest Ophthalmol Vis Sci 2004;45: 2255–62.
56. Zangwill LM, Weinreb RN, Beiser JA, Berry CC, Cioffi GA, Coleman AL, Trick G, Liebmann JM, Brandt JD, Piltz-Seymour JR, Dirkes KA, Vega S, Kass MA, Gordon MO. Baseline topographic optic disc measurements are associated with the development of primary open-angle glaucoma: the Confocal Scanning Laser Ophthalmoscopy Ancillary Study to the Ocular Hypertension Treatment Study. Arch Ophthalmol 2005;123:1188–97.
57. Alencar LM, Bowd C, Weinreb RN, Zangwill LM, Sample PA, Medeiros FA. Comparison of HRT-3 glaucoma probability score and subjective stereophotograph assessment for prediction of progression in glaucoma. Invest Ophthalmol Vis Sci 2008;49:1898–906.
58. Chauhan BC, McCormick TA, Nicolela MT, LeBlanc RP. Optic disc and visual field changes in a prospective longitudinal study of patients with glaucoma: comparison of scanning laser tomography with conventional perimetry and optic disc photography. Arch Ophthalmol 2001;119:1492–9.
59. Medeiros FA, Leite MT, Zangwill LM, Weinreb RN. Combining structural and functional measurements to improve detection of glaucoma progression using Bayesian hierarchical models. Invest Ophthalmol Vis Sci 2011;52:5794–803.
60. Leung CK, Cheung CY, Weinreb RN, Qiu K, Liu S, Li H, Xu G, Fan N, Pang CP, Tse KK, Lam DS. Evaluation of retinal nerve fiber layer progression in glaucoma: a study on optical coherence tomography guided progression analysis. Invest Ophthalmol Vis Sci 2010;51: 217–22.
61. Leung CK, Liu S, Weinreb RN, Lai G, Ye C, Cheung CY, Pang CP, Tse KK, Lam DS. Evaluation of retinal nerve fiber layer progression in glaucoma a prospective analysis with neuroretinal rim and visual field progression. Ophthalmology 2011;118:1551–7.
62. Wollstein G, Schuman JS, Price LL, Aydin A, Stark PC, Hertzmark E, Lai E, Ishikawa H, Mattox C, Fujimoto JG, Paunescu LA. Optical coherence tomography longitudinal evaluation of retinal nerve fiber layer thickness in glaucoma. Arch Ophthalmol 2005;123:464–70.
63. Leung CK, Ye C, Weinreb RN, Cheung CY, Qiu Q, Liu S, Xu G, Lam DS. Retinal nerve fiber layer imaging with spectral-domain optical coherence tomography a study on diagnostic agreement with Heidelberg Retinal Tomograph. Ophthalmology 2010;117:267–74.

Gadi Wollstein
UPMC Eye Center, Department of Ophthalmology
University of Pittsburgh School of Medicine
203 Lothrop Street
Eye and Ear Institute, Suite 834
Pittsburgh, Pennsylvania 15213
e-mail: wollsteing@upmc.edu